SYNERGY BETWEEN REMOTE SENSING AND SEISMIC METHODS: PATH CALIBRATION

Sidao Ni[1], Risheng Chu[2], Hong K. Thio[1], Arben Pitarka[1], and Donald V. Helmberger[2]

URS Group, Inc.[1] and California Institute of Technology[2]

Sponsored by National Nuclear Security Administration

Contract No. DE-AC52-03NA99505
Proposal No. BAA03-72

ABSTRACT

In previous reports, we have concentrated on validating ground truth locations by modeling extended faults with combined Interferometric Synthetic Aperture Radar (InSAR) and waveform inversions and using various combinations of seismic data at all ranges. The final task of this project involves combining the ground-truth (GT) events from the community to validate paths at all distances for regions of interest. These calibrations can then be used to address higher order source parameters (directivity) and low yield explosions. As the recent Korean shot demonstrated, we can probably expect to have a small set of teleseismic, far-regional and regional data to analyze in estimating the yield of an event. Since stacking helps to bring signals out of the noise, it becomes useful to conduct comparable analyses on neighboring events, explosions or earthquakes. If these auxiliary events have accurate locations, moments, and source descriptions, we have a means of directly comparing effective source strengths.

We now have over 30 events with well determined locations, by cluster analysis, local arrays, and/or INSAR, and source parameters. Many of these events have the Cut-And-Paste (CAP) methodology applied, where sections of synthetic seismograms are allowed to shift in time relative to the data in order to account for path corrections. The method has been shown to be greatly improved at higher frequency (2 to .5 Hz) by adding amplitude corrections, CAP+, and constructing site-responses. We demonstrate that both far-regional containing triplications and teleseismic waveform data can be used effectively to retrieve source parameters with such corrections. These corrections can be larger than 10 at many stations which has prevented the inversion of small events in the past. Moreover, certain paths prove difficult to calibrate because of rapidly varying waveforms while some prove stable, i.e., ABKT, and ANTO. We present calibration results for both 1D and 3D models for these selected paths where source parameters are demonstrated to agree with regional results.

Report Documentation Page

Form Approved
OMB No. 0704-0188

1. REPORT DATE	2. REPORT TYPE	3. DATES COVERED
SEP 2008		**00-00-2008 to 00-00-2008**

4. TITLE AND SUBTITLE	5a. CONTRACT NUMBER
Synergy Between Remote Sensing and Seismic Methods: Path Calibration	5b. GRANT NUMBER
	5c. PROGRAM ELEMENT NUMBER
6. AUTHOR(S)	5d. PROJECT NUMBER
	5e. TASK NUMBER
	5f. WORK UNIT NUMBER
7. PERFORMING ORGANIZATION NAME(S) AND ADDRESS(ES) **URS Group Inc,600 Montgomery Street,San Francisco,CA,94111-2728**	8. PERFORMING ORGANIZATION REPORT NUMBER
9. SPONSORING/MONITORING AGENCY NAME(S) AND ADDRESS(ES)	10. SPONSOR/MONITOR'S ACRONYM(S)
	11. SPONSOR/MONITOR'S REPORT NUMBER(S)

12. DISTRIBUTION/AVAILABILITY STATEMENT
Approved for public release; distribution unlimited

13. SUPPLEMENTARY NOTES
Proceedings of the 30th Monitoring Research Review: Ground-Based Nuclear Explosion? Monitoring?Technologies, 23-25 Sep 2008, Portsmouth, VA sponsored by the National Nuclear Security Administration (NNSA) and the Air Force Research Laboratory (AFRL)

14. ABSTRACT
see report

15. SUBJECT TERMS

16. SECURITY CLASSIFICATION OF:			17. LIMITATION OF ABSTRACT	18. NUMBER OF PAGES	19a. NAME OF RESPONSIBLE PERSON
a. REPORT **unclassified**	b. ABSTRACT **unclassified**	c. THIS PAGE **unclassified**	**Same as Report (SAR)**	**10**	

OBJECTIVES

The International Monitoring System has been concentrating on locating and estimating source parameters by following two strategies; (1) calibration-based and (2) model-based. The first relies on path calibration from well-located events while the second attempts to estimate the source properties from a well-developed 3D earth models. The focus of this report is to use our GT events in conjunction with efforts from our colleagues to establish a master-set of simple events with well determined source mechanisms and P-wave segments sampling the upper mantle transition zone. This collection can then be used effectively to calibrate specific paths or refine 3D earth structures in Southeast Asia.

RESEARCH ACCOMPLISHED

The importance of triplications or natural focusing produced by the earth is easily observed by examining observations from the recent Korean test and neighboring earthquakes, Kim (1995), as displayed in Figure 1. Note that the explosion signal is well above the noise that is predicted by synthetics, although the true nature of this sample of the mantle is not well known with only a prediction given here. Similarly, the PKP triplication again displays a strong signal for the explosion. The core phases are well known relative to the upper mantle triplications where individual arrivals prove difficult to isolate.

Although there have been many attempts at performing such tasks, they have not been very successful because of the complexity involved with seismograms at distances of less than 30°. Thus, most global tomography studies use P-data beyond 30° and PP beyond 60°, etc. It appears that the main difficulty is that depth phases from crustal events arrive on top of the triplications and make it difficult to identify secondary arrivals when only a collection of individual events are assembled into a record section. Fortunately, dense arrays display very clear triplications, Figure 2, and allow some systematic approaches to be developed in refining structures and establishing path corrections. The first is that we must have clear identifications of depth phases and accurate source characterization, and second, we must either correct for complicated source histories or eliminate such events from consideration.

We started with 1,720 events with CMTs Mw > 5 within our study area, Figure 2A, and examined their teleseismic waveforms as in Figure 2B. After testing forward synthetics, we only accepted those events that allowed clear depth phases pP and sP at several stations at different azimuths. If the Harvard centroid moment tensor (CMT) had roughly the right mechanism, we simply adjusted the depth determination to fit the deconvolved records as displayed in Figure 2B. Only 504 events remained after this analysis, which we will refer to as Master Events. A comparison of these depths is given in Figure 3 along with maps of CMT and National Earthquake Information Center (NEIC) depths as color coded (Figure 4). Note that many of the events in the region of Iran have been relocated at shallower depths. This means that their origin times need to be adjusted when developing travel time correction surfaces.

The source durations were deconvolved and stored along with the other source parameters to establish a master set. Next, we collected a large sample of P-wave recordings at all ranges of less than 30° (over 21,000 30s segment for these events). We used a library of triplication models to identify turning depths of the various arrivals. After relocation by gathering GT information from the community, we can test existing 3D earth models and perform tomographic images of individual triplication branches. With refined triplication models we can attempt source inversion using the CAP (Cut and Paste) methodology to all ranges.

Mapping Triplications

Next, we examined the recording of these Master Events at more than 300 stations in the ranges less than 30°, including those from the global seismological network, KNET, KZNET, and CNDSN (Chinese National Digital Seismic Network). We also included all the PASSCAL-type data; Sino-US (XC), INDEPTH II & III (XR), Nanga Parbet (XG), GHENGIS (XW), Tarim (XM), HIMNT (YL), BHUTAN (XA), Namche Barwa (XE), MIT-China (YA) and the Sochuan (XS). Over 20,000 P-waves were collected.

Record sections were assembled from this collection with common depth points as displayed in Figure 5, and some preliminary 1D modeling, Chu (2008). Even though these synthetics involve several different mechanisms and depths, the triplicated branches become apparent as indicated by the dotted lines. The fast structure above the 410 km discontinuity is interpreted as a flat lying slab, Chu and Zhu (2008).

Regional Travel-Time Samples

The upper-mantle samples from the entire collection is displayed in Figure 6A with travel-time depth anomalies plotted in Figure 6B displaying the large variation along an India-Tarim Basin cross-section AB. The AB line is denoted in Figure 7A. Note that negative travel-time residuals (blue) indicate that the velocities around the turning points are faster than those in iasp91, while positive residuals (red) suggest slow velocity anomalies. Negative residuals above the 410 appear to dominate most of the cross-section except beneath the northern edge of the Tibetan Plateau. A sharp boundary appears at the northern edge of the Tarim Basin at depths greater than 200 km, but ends at the 410 discontinuity. This structure is similar to detached slab segments that have been imaged beneath the Western United States. A relatively slow patch occurs at about Lon (85°), Lat (36°) which appears to be a localized up-welling, which is also seen in receiver functions, Kind et al (2002).

Travel-time residuals below the 410 km are relatively small beneath the entire region, except directly beneath the Southern edge of the Tibet. This feature can be seen in some of the tomographic images (Li et al., 2006), but is weaker in our data set.

CONCLUSIONS AND RECOMMENDATIONS

In this study, we have refined the source properties over 500 events by modeling P, pP and SP at teleseismic distances. Multiple arrivals on these records have been identified, delineating distinct travel paths. Then pulses can be used directly in comparing neighboring events or assembled to refine existing 3D earth models. The timing delays can be used directly in tomographic style and added to existing files or waveform segments matched against 3D synthetics.

Unfortunately, most of the recent events studied by means of InSAR, cluster analysis and local arrays have not been included in the above dataset. Over 30 events in IRAN now have well determined locations. Many of these events have the CAP methodology applied, where sections of synthetics seismograms are allowed to shift in the time relative to the data in order to a recount for path corrections. We recommend that all these events be added to the above collections. Moreover, we recommend performing the CAP analyses at all distances including the above collection where site-corrections are applied (CAP +, Tan and Helmberger, 2006). This will allow source estimations using a complete set of waveforms. Moreover, solutions become possible even with a sparse network (Thio et al, 1999).

REFERENCES

Chu, R (2008). Upper mantle velocity structure beneath the Tibetan Plateau from triplicated seismic P waveforms, *PhD Thesis*, Saint Louis University.

Chu, R. and L Zhu (2008). Detached Eurasian mantle lithospheric remnants beneath the Tibetan plateau inferred from triplicated P waveforms, *JGR, in preparation.*

Chu, R., S Ni and D.V. Helmberger (2008). Mapping lateral variation in upper mantle triplications beneath the Eastern Pacific Margins, *in preparation.*

Kim, S. K., 1995. A study on the crustal structure of the Korean Peninsula (in Korean), *J. Geol. Soc. Korea* 31: 393–403.

Kind, R., Yuan, X., Saul, J., Nelson, D., Sobolev, S. V., Mechie, J., Zhao, W., Kosarev, G., Ni, J., Achauer, U., Jiang, M. (2002). Seismic images of crust and upper mantle beneath Tibet: evidence for Eurasian plate subduction, *Science* 298: 5596, 1219–1221.

Li, C, R.D. van der Hilst, and N.M. Toksoz (2006). Constraining spatial variation in P wave velocity in the upper mantle beneath SE Asia, *Phys. Earth Planet. Inter.* 154: 180–195.

Ni, S., Ding X. and D.V. Helmberger (2000). Constructing synthetics from deep earth tomographic models, *Geophys. Journ. Int.* 140: (1), 71–82.

Ni, S., Cormier V. and D.V. Helmberger (2003). A comparison of synthetic seismograms for 2D structures: Semianalytical versus numerical, *Bull. Seis. Soc. Am.* 93: (6), 2752–2757.

Ni, S., A. Pitarka, D.V. Helmberger, (2008). Short-period Synthetics for 3D models, Numerical vs. Analytical, *Seis. Res. Lett.* 79: .2, p. 298.

Tan, Y and D.V. Helmberger (2007). A new method for determining small earthquake source parameters using short-period P waves, *Bull., Seism. Soc. Am*. 97: 1176–1195.

Thio, H. K., Song, X, Saikia, C. K., Helmberger, D. V., and Woods, B.B. (1999). Seismic source and structure estimation in the western Mediterranean using a sparse broadband network, *Journ. Geophys. Res.* 104:(B1) pp. 845–861.

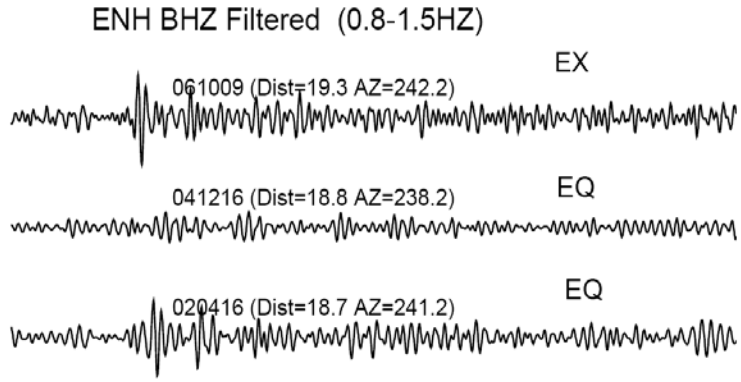

Figure 1A. P waves at upper mantle triplication distances recorded at station ENH for three events. Event 041216 shows weaker amplitude probably due to its source mechanism.

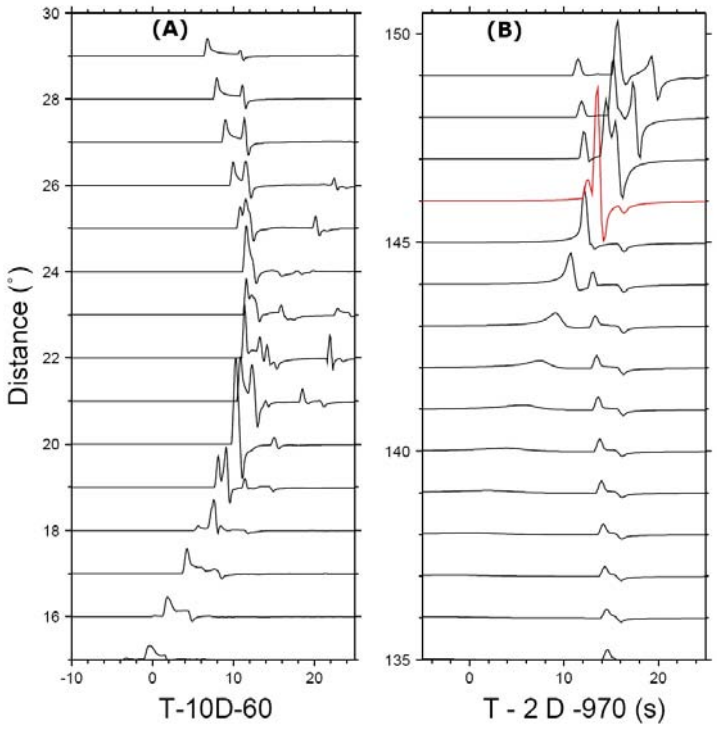

Figure 1B. (A) Synthetic P waveforms at upper mantle triplication distances based on 3D tomography model by Grand (2002) with the WKM algorithm (Ni et al., 2000). Around distances of 19-20 degrees, P waves are substantially stronger because of constructive interference of various triplication branches. (B) Synthetic PKIKP/PKPab/bc waveforms for PREM. Note that PKP is very strong around 146 degrees (green trace) since it is close to B-caustic.

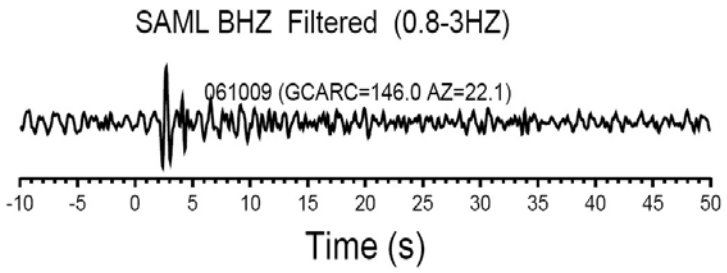

Figure 1C. The 061009 explosion observed at station SAML at a distance of 146 degrees.

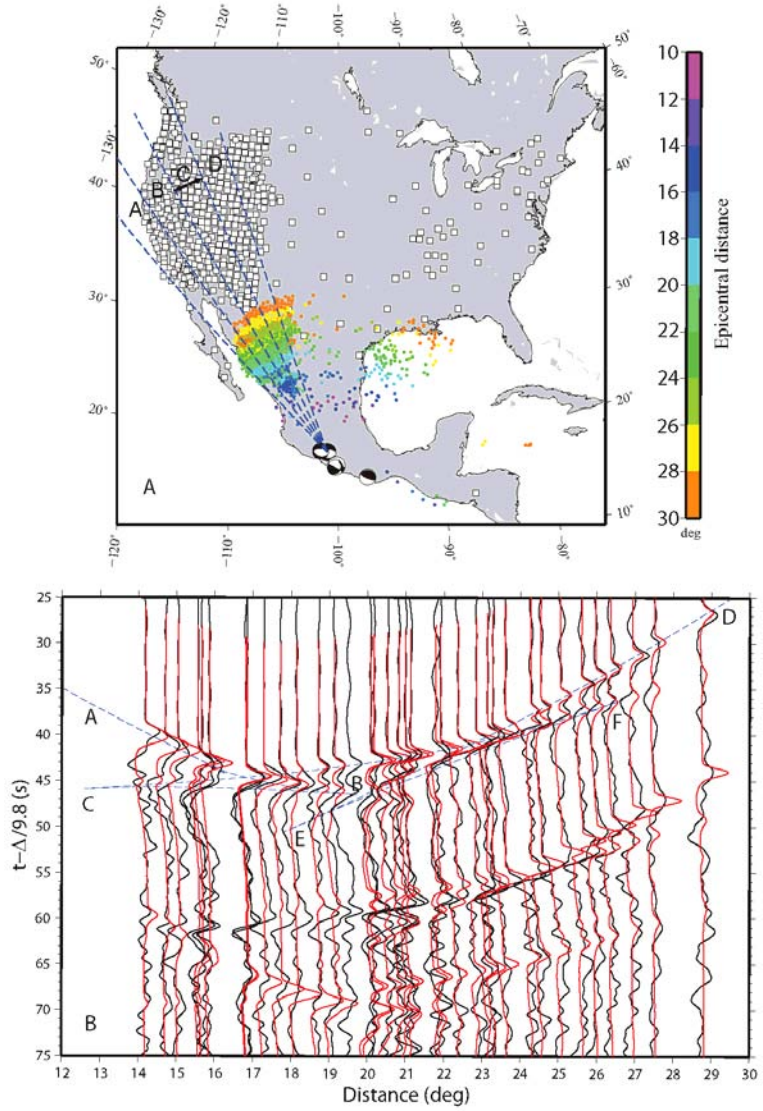

Figure 2. Upper-mantle triplications observed on the US Array of an event beneath Mexico (top). The model is a modification of GCA (Chu and Helmberger, 2008). The event is at a depth of 65 km so that the depth phases are apparent. For shallow events, their depth phases interfere with the various branches of the two triplications caused by the 410 and 660 km discontinuities, respectively. In this case, the P-wave portion is isolated, so that we can easily identify the AB branch which is the first arrived at distances less than 17°, the CD branch from 18° to 22°, and the EF branch beyond 24°, as denoted by the dotted lines (bottom).

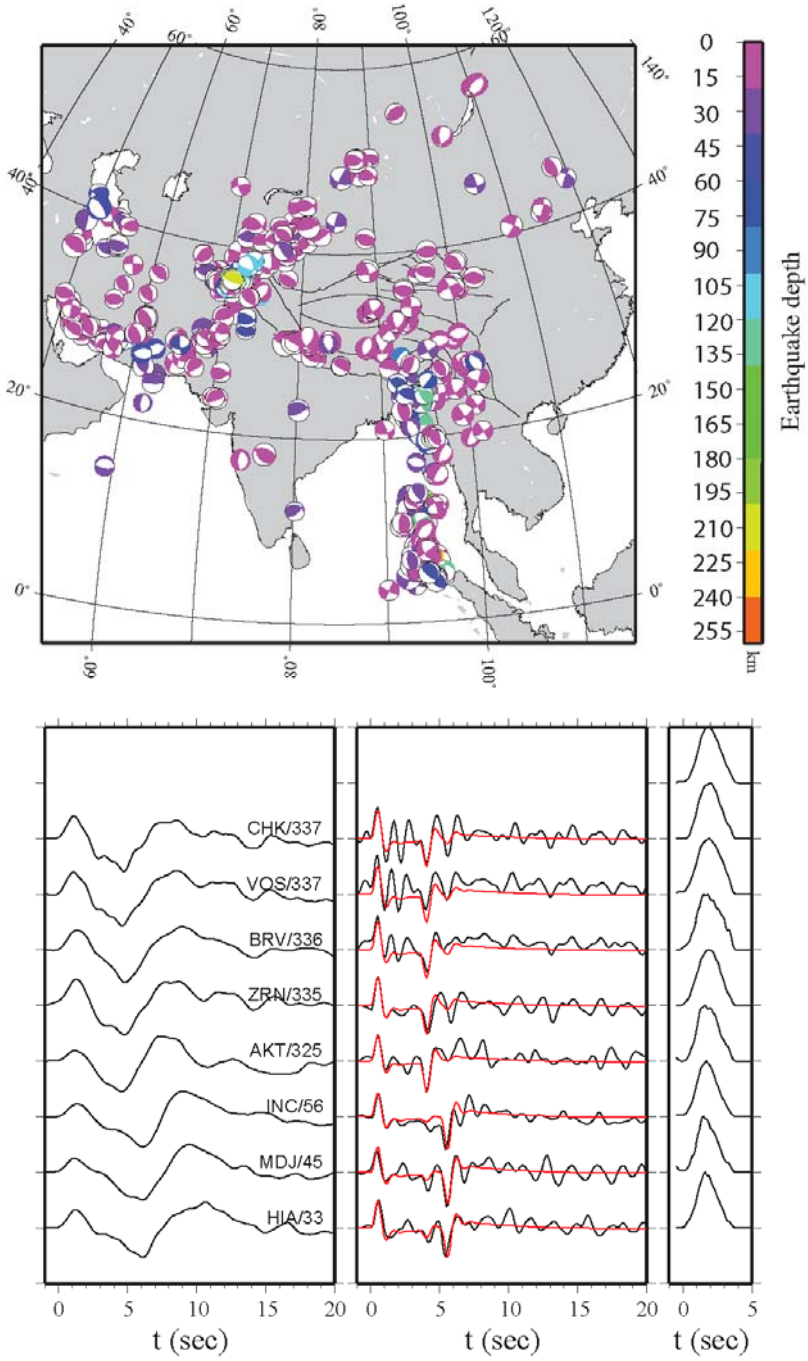

Figure 3. Master events with the verified mechanisms and refined depths using teleseismic modeling (top). Only events shallower than 250 km are plotted in color-code. The bottom panel shows an example of modeling depth phases for a shallow event (d=11km) and derived source time function obtained by deconvolutions [Chu et. al, 2008]. Note that the bottom three traces display a strong sP relative to those above.

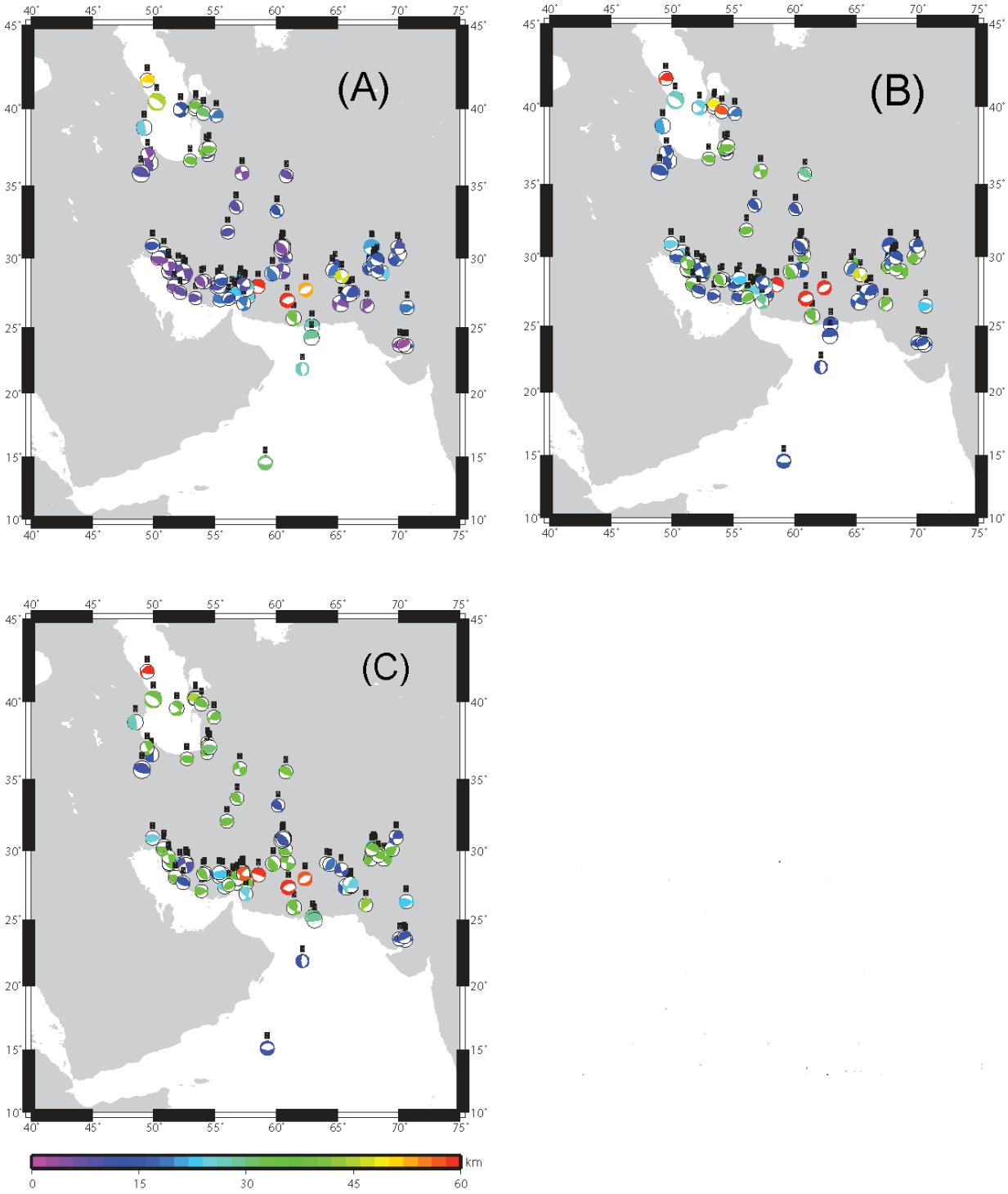

Figure 4. Comparison of the earthquake depths estimated for the region of Iran using the technique by Chu et al. (2008). Note that most of the events in the interior of Iran are distinctly shallower in our results (A) vs. the depths from the CMT (B) and NEIC catalogs (C), although some of the events beneath the Captain Sea are deeper.

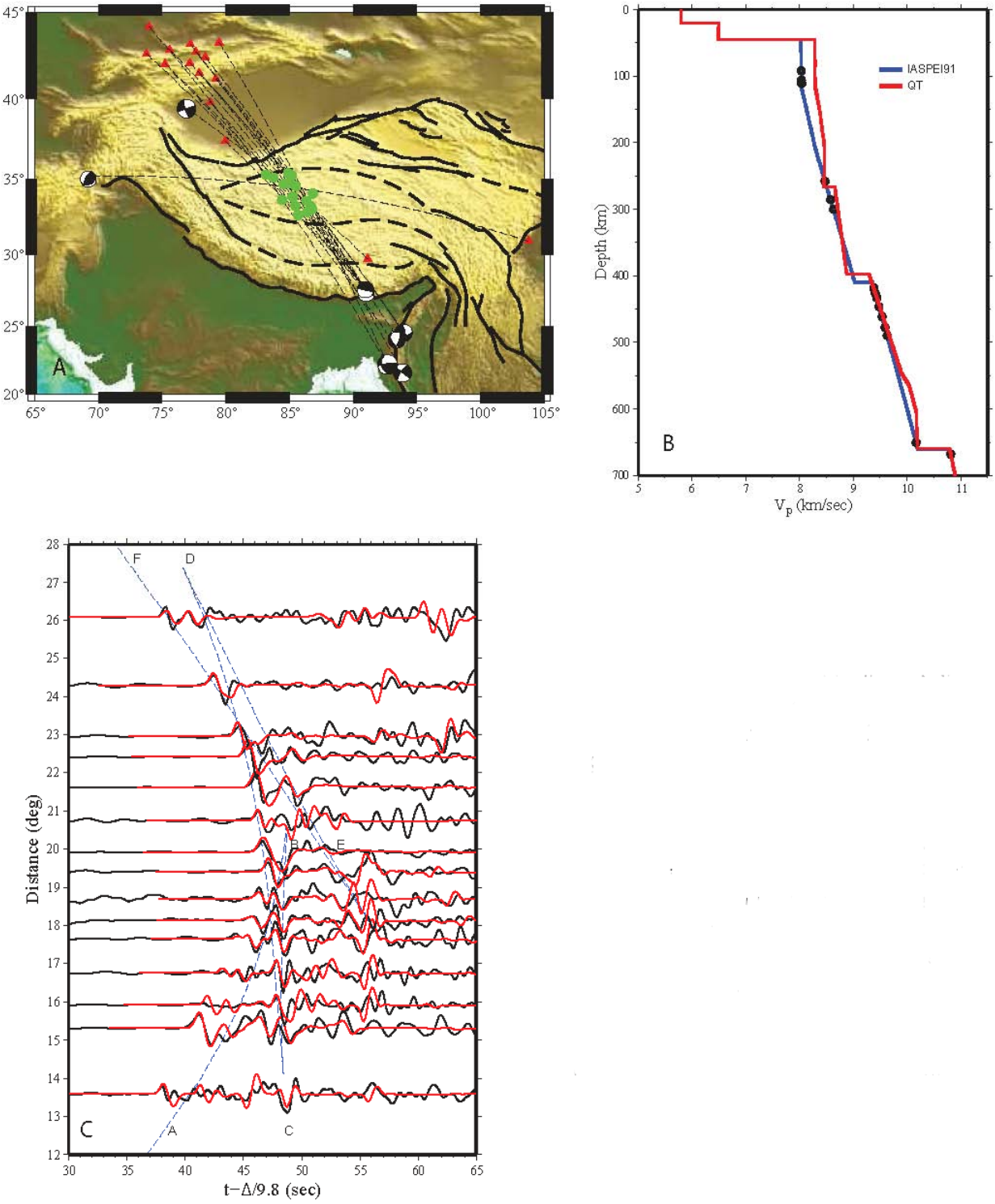

Figure 5. Modeling triplications at a common depth sampling the upper mantle beneath the Qiangtang province of Central Tibet. Figure 5A shows the event-station pairs and turning points (green dots) of seismic rays in Figure 5C. The black dots in Figure 5B represent the bottoming depths of the various ray paths assuming a 1D model (iasp91). Thus, the nearest event provides the smallest range (13.7 deg) while the most distant event (26.1 deg.) produces the deepest sample. The best fitting model (QT) is displayed in Figure 5B in red with the associated waveform fits in Figure 5C. The various traces involve individual source parameters.

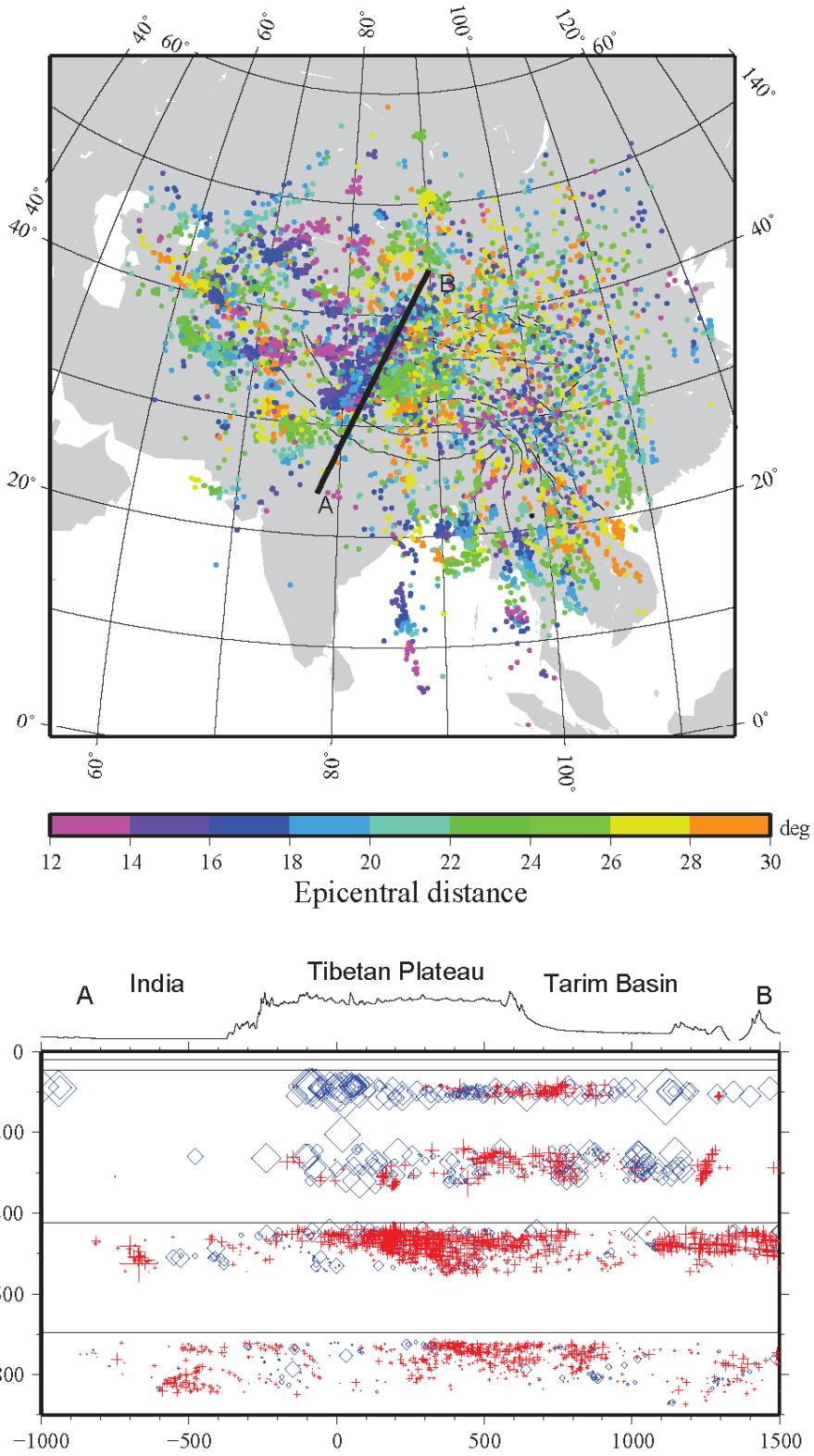

Figure 6. A map displaying the mid-points between each event-station pair involving 11,306 samples (top). The color scale shows the epicentral distance for each sample, which corresponds to its turning depth. The profile AB is a cross section in western Tibet. Travel time residuals relative to iasp91 along AB (bottom) with negative values (blue) indicating relatively fast paths (high velocities). See Figure 7 for scale of differential times.

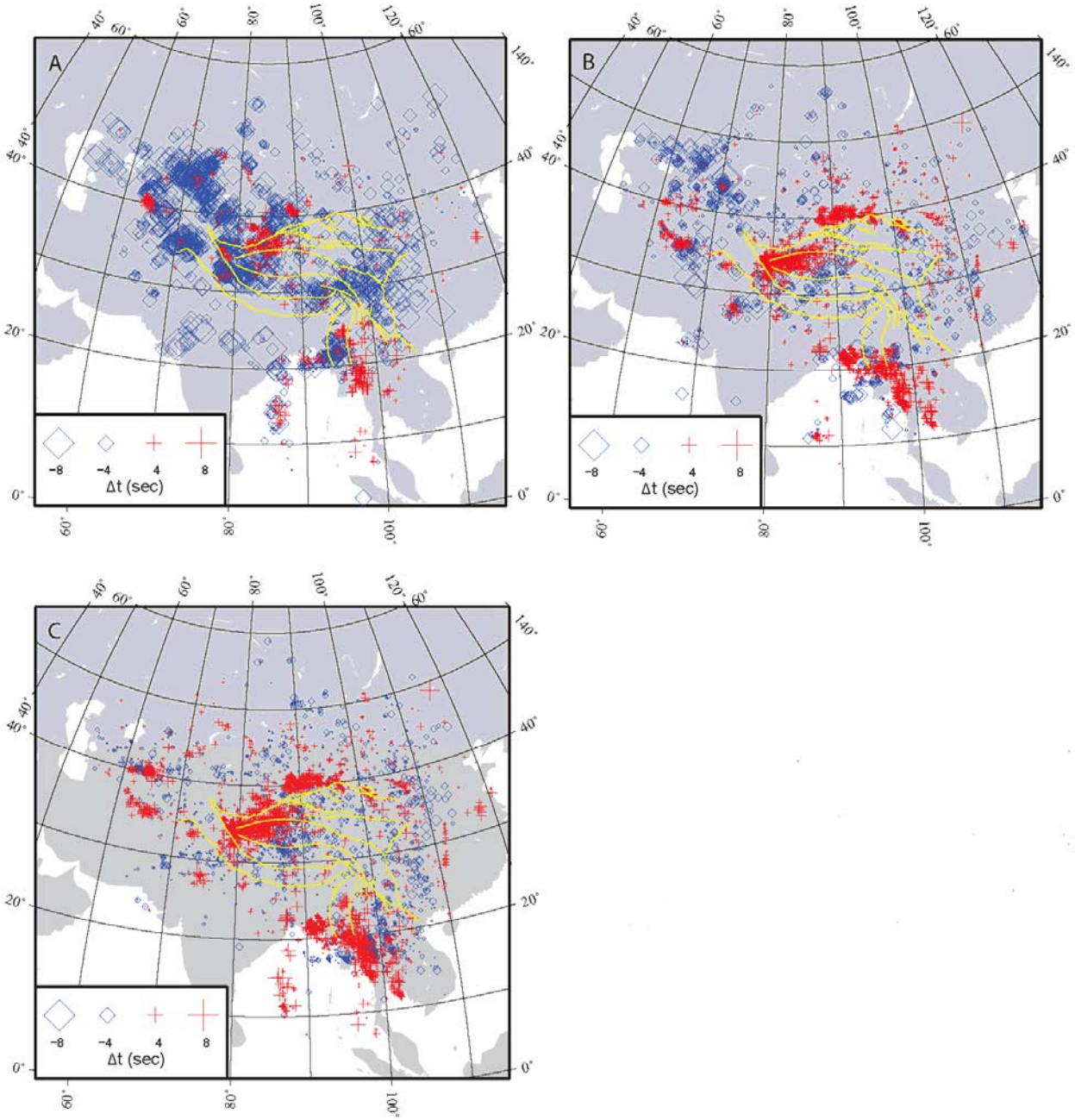

Figure 7. Display of travel time anomalies at various depths beneath Southeast Asia. The delays are plotted relative to branch's. Figure 7(A) shows the delays for those rays sampling above the 410 km discontinuity. The CD branch sampling in the transition zone, 410 to 660 km, are presented in Figure 7(B) and below 660 km given in Figure 7(C).